

Supporting information for Observation of a biexciton Wigner molecule by fractional optical Aharonov-Bohm oscillations in a single quantum ring

Hee Dae Kim,^{†,‡} Rin Okuyama,[¶] Kwangseuk Kyhm,^{*,§,†} Mikio Eto,[¶] Robert A. Taylor,^{*,‡} Aurelien L. Nicolet,^{||} Marek Potemski,^{||} Gilles Nogues,[§] Le Si Dang,[§] Koo-Chul Je,[⊥] Jongsu Kim,[#] Ji-Hoon Kyhm,[@] Kyu Hyoek Yoen,[@] Eun Hye Lee,[@] Jun Young Kim,[@] Il Ki Han,[@] Wonjun Choi,[@] and Jindong Song[@]

[†]*Department of Opto and Cognomechatronics, Department of Physics Education, Pusan Nat'l University, Busan 609-735, South Korea*

[‡]*Clarendon Laboratory, Department of Physics, University of Oxford, Oxford, OX1 3PU, U.K*

[¶]*Faculty of Science and Technology, Keio University, 3-14-1 Hiyoshi, Kohoku-ku, Yokohama 223-8522, Japan*

[§]*Department of NANOScience, Institut Néel, CNRS, rue des Martyrs 38054, Grenoble, France*

^{||}*Laboratoire National des Champs Magnetiques Intenses, CNRS-UJF-UPS-INSA, F-38042, Grenoble, France*

[⊥]*College of Liberal Arts and Sciences, Anyang University, Gyeonggi-do 430-714, South Korea*

[#]*Department of Physics, Yeungnam University, Gyeonsan 712-749, South Korea*

[@]*Center for Opto-Electronic Convergence Systems, KIST, Seoul, 136-791, South Korea*

E-mail: kskyhm@pusan.ac.kr; r.taylor1@physics.ox.ac.uk

Supporting information-1: Experimental Method

The nano quantum rings (NQRs) were grown in Riber Compact21 MBE system. After thermal removal of any surface oxide on the GaAs under an As tetramer ambience of 620°C, a ~ 100 nm-thick GaAs buffer layer was grown at 580°C. 20 pairs of (61.35 nm-thick AlAs and 53.2 nm-thick $\text{Al}_{0.31}\text{GaAs}$) and 53.2 nm-thick $\text{Al}_{0.31}\text{GaAs}$ were grown successively. The substrate temperature was then cooled to 310°C and the supply of As tetramer was disconnected until the partial pressure of As and the pressure of the main chamber became less than 1×10^{-11} Torr and 1.5×10^{-9} Torr, respectively. Ga metal was introduced on the substrate in this clean state of the chamber, equivalent to 1 monolayer of GaAs. In this state, the density of Ga droplets was $\sim 7 \times 10^8 \text{ cm}^{-2}$. After As tetramer introduction at a beam equivalent pressure of 1.25×10^{-7} Torr at 200°C, the Ga droplets changed into GaAs quantum ring structures. A 53.2 nm-thick layer of $\text{Al}_{0.31}\text{GaAs}$ was then grown on the rings. Finally, the whole structure was annealed in the chamber under an As tetramer ambient of beam equivalent pressure of 3.00×10^{-6} Torr at 600°C for 1 hour.

The micro-PL spectrum of a single NQR was measured at 4.2 K using a confocal arrangement, where the PL spectrum was measured by charge coupled device under the excitation of frequency-doubled (400 nm) Ti:sapphire laser pulse (120 fs pulse duration at a 80 MHz repetition rate). Magneto-PL from a single NQR was also performed in a resistive DC magnet (52 mm-bore diameter), where a miniaturised optical alignment system was installed and the sample position was controlled by a piezoelectric stage. Excitation by a continuous-wave Ar^+ -ion laser (488 nm) was introduced to the sample through a multi-mode fiber, and the PL was detected through another single-mode optical fiber.

Supporting information-2: Identification of charged excitons and biexcitons in a single NQR

While the optical AB effect terminology is often used to present the energy oscillations in the exciton PL spectrum, charged excitons (M. Bayer *et al.*, Phys. Rev. Lett. 90, 186801 (2003)) and biexcitons (R. Okuyama *et al.*, Phys. Rev. B 83, 195311 (2011)) can also result in novel energy oscillations in the PL spectrum. In the case of quantum dots, either negatively or positively charged excitons are often measured. For increasing the excitation intensity, charged excitons also dominate along with biexcitons in the PL spectrum, where both the PL intensity increases super-linearly with excitation intensity. As a preliminary work, we have identified charged excitons and biexcitons in terms of the excitation power dependence and time-resolved PL.

As shown in S-Fig. 1(a), additional PL peaks arise near the neutral exciton (X) with increasing the excitation intensity. In S-Fig. 1(b), the integrated PL intensity of the additional PL peaks was plotted for excitation intensity (I), whereby the power factor (α) for the excitation ($\sim I^\alpha$) were obtained. While the integrated PL intensity of X increases linearly with excitation intensity ($\alpha \sim 0.99$), the XX and two charged excitons increase super-linearly with $\alpha \sim 2.02$ (XX), ~ 1.59 (X_2^*), and ~ 1.49 (X_1^*) respectively. Because our samples were undoped, charged excitons were rarely observed unless the excitation intensity was strong enough to generate XXs. Therefore, the charged excitons are possibly generated via the XX decay. As shown in S-Fig. 1(c), normalised time-resolved PL spectra from X, XX, X_1^* , and X_2^* were compared under an excitation power of 1.9 kWcm^{-2} . As the carriers are generated by strong excitation, XXs dominate earlier than Xs during the rising time of the TR-PL. However, dissociation of the XXs occurs with a decay time of $\tau_{XX} \sim 370 \text{ ps}$, which is significantly shorter than the decay time of Xs ($\tau_X \sim 820 \text{ ps}$). Since the population of Xs can also be enhanced by the dissociation of XXs, the maximum TR-PL intensity of Xs appears later than that of XXs, and the X population is saturated transiently up to $\sim 250 \text{ ps}$. Meanwhile,

either positively or negatively charged excitons can be generated. As a result, the maximum population of the charged excitons is seen later than that of Xs. Nevertheless, the decay times of the charged excitons ($\tau_{X_1^*} \sim 880$ ps for X_1^* and $\tau_{X_2^*} \sim 890$ ps for X_2^*) are comparable to that of the X. On the other hand, it should be noted that the XX binding energy in S-Fig. 1(a) is sub meV, which is smaller than a few meV for the XX binding energy in GaAs quantum dots (30 – 40 nm in radius) (M. Ikezawa *et al.*, Phys. Rev. B 73, 125321 (2006) and J. W. Luo and A. Zunger, Phys. Rev. B 84, 235317 (2011)). While Xs are likely to be localised in the anisotropic ring structure in the absence of a magnetic field, the wavefunction of XX can be more extended. In this case, two kinds of XXs are possible. One is a localised XX, which consists of two Xs localised in the same crescent-like structure. Another one is an extended XX, where separate Xs are located in two different crescent-like structures. This is similar to the XX in a coupled-dot-molecule. In the latter case, the extended XX binding energy should be sub-meV (Ta-Chun Lin *et al.*, Phys. Rev. B 80, 081304 (2009)). For the localised XX in a NQR, the XX binding energy was observed to be ~ 5 meV from the PL spectrum near 1.816 eV (H. D. Kim *et al.*, Appl. Phys. Lett. 102, 033112 (2013)). Because the extended XX is advantageous for circumferential phase coherence, we found a particular NQR with the sub-meV XX binding energy (Fig. 1(c),(e)) for the fractional optical AB oscillations.

Supporting information-3: Theoretical model with quasi 1-dimensional confinement potential for the optical Aharonov-Bohm effect

For the theoretical results given in Fig. 2(b), Fig.4(b),(c),(d), and Fig.5(a),(b), we used a model of a quasi 1-dimensional NQR, where the radial confinement is given by the finite rim width. The eigenenergy levels and the two-body density for the exciton and biexciton were

obtained by using the exact diagonalisation method, where a Coulomb interaction between the electron and the hole was also considered in the presence of an external magnetic field ($B = B\hat{z}$) applied perpendicular to the lateral xy plane of a NQR. We assumed the isotropic confinement potential as an ideal theoretical reference, whereby the anisotropy effect of a volcano-like NQR can be compared. While AB oscillations of our NQR emerge beyond a threshold magnetic field, theoretical AB oscillations begin from $B = 0$. Therefore, the theoretical results can be used as a reference to measure a magnetic field difference for the AB oscillation extremum between theory and experiment (δB), whereby the modulated AB oscillations in a real NQR is defined in this context.

We used different orbital radii of the electron (R_e) and the hole (R_h) in order to consider charge separation effects for the electron and hole, which are known to be crucial for optical AB oscillations to emerge (A. O. Govorov *et al.*, Phys. Rev. B 66, 081309 (2002), Luis G. G. V. Dias da Silva *et al.*, Phys. Rev. B 72, 125327 (2005)). In a NQR, any asymmetry of the confinement potential likely gives rise to a so-called radially polarised electron-hole pair, whereby the electron and hole rotate along the different orbits. Suppose the electron and hole are confined in an anharmonic potential along the radial direction, a wavefunction separation between the electron and hole can occur due to the mass difference and the asymmetry of the confinement potential. Additionally, there are various other effects which possibly result in a radially-polarised electron-hole pair in a NQR such as the deformation potential with a large difference in the conduction and valence bands, the strain-induced piezoelectric field, and the local electric field arising from the charge-trapped interface defects. Therefore, it is plausible to assume different orbital radii for the electrons and holes ($R_e \neq R_h$) to describe the charge separation effect. According to a recent theory, strain effects are known to localise the hole toward the ring center (V. V. Arsoski *et al.* Phys. Rev. B 87, 085314 (2013)), whereas the electron resides within the rim width. Also, in the case of an anharmonic radial confinement, tunneling towards the direction away from the ring center could be dominated by light electron. Therefore, we assumed the orbital radius of the

electron to be larger than that of the hole ($R_e > R_h$). Nevertheless, our model is still arbitrary as experimental clarification has yet to be accomplished for the separation between the electron and hole. While AB oscillations of our NQR emerge beyond a threshold magnetic field, theoretical AB oscillations begin from $B = 0$. Therefore, the theoretical results can be used as a reference to measure a magnetic field difference for the AB oscillation extremum between theory and experiment (δB), whereby the modulated AB oscillations in a real NQR is defined in this context.

Suppose N_e electrons and N_h holes are given in a single NQR, the effective mass Hamiltonian can be given by $H = H_e + H_h + V_C$,

$$H_e = \sum_{j=1}^{N_e} \left\{ \frac{[p_{e,j} + eA(r_{e,j})]^2}{2m_e} + V_e(r_{e,j}) + \frac{1}{2}E_g + g_e\mu_B S_{e,j}^z B \right\}, \quad (1)$$

$$H_h = \sum_{j=1}^{N_h} \left\{ \frac{[p_{h,j} - eA(r_{h,j})]^2}{2m_h} + V_h(r_{h,j}) + \frac{1}{2}E_g + g_h\mu_B S_{h,j}^z B \right\}, \quad (2)$$

$$V_C = \sum_{1 \leq j < k \leq N_e} \frac{e^2}{4\pi\epsilon|r_{e,j} - r_{e,k}|} + \sum_{1 \leq j < k \leq N_h} \frac{e^2}{4\pi\epsilon|r_{h,j} - r_{h,k}|} - \sum_{j=1}^{N_e} \sum_{k=1}^{N_h} \frac{e^2}{4\pi\epsilon|r_{e,j} - r_{h,k}|}, \quad (3)$$

with $A(r) = (1/2)B \times r$. H_e (H_h) is the Hamiltonian for non-interacting electrons (holes), whereas V_C describes the Coulomb interaction. m_α and g_α are the effective mass and g -factor for electrons ($\alpha = e$) and holes ($\alpha = h$), respectively. E_g , ϵ , and μ_B are the band gap, the dielectric constant, and the Bohr magneton, respectively. We use $m_e = 0.067m_0$, $m_h = 0.51m_0$, and the effective Bohr radius $a_B = 4\pi\epsilon\hbar^2/(\mu e^2) = 12$ nm with $\mu^{-1} = m_e^{-1} + m_h^{-1}$, for GaAs. The g -factors for electrons (g_e) and holes (g_h) are associated with the observable excitonic g -factor ($g_X = g_e - g_h = -1.3$). The anharmonic confinement potential energy $V_\alpha(r)$ is given by (C. González-Santander *et al.*, Phys. Rev. B 84, 235103 (2011))

$$V_\alpha(r) = \frac{\hbar^2\lambda_\alpha^2}{2m_\alpha r^2} + \frac{1}{2}m_\alpha\omega_\alpha^2 r^2. \quad (4)$$

Using $\lambda_\alpha = (1/2)(R_\alpha/W_\alpha)^2$ and $\omega_\alpha = \hbar/(2m_\alpha W_\alpha^2)$, this can be approximated as

$$V_\alpha(r) = \frac{\hbar^2}{2m_\alpha W_\alpha^2} \left[\frac{1}{4} \left(\frac{R_\alpha}{W_\alpha} \right)^2 + \left(\frac{r - R_\alpha}{W_\alpha} \right)^2 + \mathcal{O} \left(\frac{r - R_\alpha}{W_\alpha} \right)^3 \right]. \quad (5)$$

Therefore, $V_{\alpha=e,h}(r)$ describes a quasi 1-dimensional isotropic confinement potential energy with orbital radius R_α and confinement width W_α . Since R_e and R_h are much larger than the atomic scale, the effective mass approximation is still valid, and we considered only the heavy-hole state, which means the mixing between the heavy-hole and light-hole states is ignored.

Note that $V_{\alpha=e,h}(r)$ is a lateral confinement potential energy. In order to explain the energy of the X PL spectrum near ~ 1.732 eV, the vertical confinement energy also needs to be considered. Because the lateral size of our NQR is larger than the vertical size, similar to the case of a pancake, the vertical confinement energy can be separated according to the adiabatic approximation. The so-called adiabatic potential obtained through this approximation corresponds to $V_{\alpha=e,h}(r)$, which also represents the morphology of a NQR. Therefore, the vertical confinement energy gives an energy offset of $V_{\alpha=e,h}(r)$ with respect to the conduction and valence band edge of bulk GaAs, respectively. For ~ 10 , nm height of our NQR, the total vertical confinement energy for an electron-hole pair is ~ 194.1 meV. With rough estimation of the Coulomb interaction by $\frac{e^2}{4\pi\epsilon|R_e-R_h|} \sim 6$ meV, the energy of the X PL spectrum near ~ 1.732 eV can be explained. Therefore, this is the case that both lateral and vertical confinement energy are larger than the Coulomb interaction. However, our calculation is not the case of single-particle states with Coulomb corrections. The many-body correlation is fully taken into account. We expanded the many-body states by the single-particle states. In this case, a large number of the single-particle states are required for calculation to converge. We have confirmed that the truncation error becomes negligibly small with few thousands of the single-particle states.

For the single-particle states ($H_{\alpha=e,h}$) of a NQR in the presence of an external magnetic

field, the eigenenergy and eigenfunction can be obtained analytically (W. C. Tan and J. C. Inkson, *Semicond. Sci. Technol.* 11, 1635 (1996)) as

$$E_{\alpha,n,m} = \frac{\hbar^2}{2m_\alpha W_\alpha^2} \left\{ \frac{1}{2} \left[\left(\frac{R_\alpha}{W_\alpha} \right)^4 + m^2 \right]^{1/2} + 2n + 1 \right\} \left[1 + 4 \left(\frac{W_\alpha}{R_\alpha} \right)^4 \phi_\alpha^2 \right]^{1/2} - \frac{\hbar^2 \phi_\alpha m}{m_\alpha R_\alpha^2} + \frac{1}{2} E_g, \quad (6)$$

$$\psi_{\alpha,n,m}(r) = \left[\frac{n!}{\pi \Gamma(\mu_{\alpha,m} + n + 1)} \right]^{1/2} \frac{1}{\Omega_\alpha} \left(\frac{r}{\Omega_\alpha} \right)^{\mu_{\alpha,m}} e^{-r^2/(2\Omega_\alpha^2)} P_n^{\mu_{\alpha,m}} \left(\frac{r^2}{\Omega_\alpha^2} \right) e^{im\theta}, \quad (7)$$

for angular momentum $m = 0, \pm 1, \pm 2, \dots$ and radial quantum number $n = 0, 1, 2, \dots$ with $P_j^k(x)$ being the associated Laguerre polynomials and

$$\phi_\alpha = \mp \frac{\pi R_\alpha^2 B}{h/e}, \quad \mu_{\alpha,m} = \frac{1}{2} \left[\left(\frac{R_\alpha}{W_\alpha} \right)^4 + 4m^2 \right]^{1/2}, \quad \Omega_\alpha = \sqrt{2} W_\alpha \left[1 + 4 \left(\frac{W_\alpha}{R_\alpha} \right)^4 \phi_\alpha^2 \right]^{-1/4}. \quad (8)$$

Using these states, we diagonalised the Hamiltonian H numerically, and the matrix elements of the Coulomb interaction were evaluated analytically by the use of the multipole expansion (R. Okuyama *et al.*, *Phys. Rev. B* 83, 195311 (2011)). As $(R_\alpha/W_\alpha)^2 \gg 1$, we only consider the states with $n = 0$. The states with $n > 0$ hardly modify the calculated results.

Finally, the exciton eigenenergies ($E_X^L(B)$) for different exciton orbital angular momenta (L) were obtained as a function of the external magnetic field (B). When the excitonic Zeeman effect is considered with the exciton g-factor (g_X), the two exciton PL peak energy of spin-parallel ($E_X^{\sigma^+}$) and anti-parallel ($E_X^{\sigma^-}$) can be given as

$$E_{X-PL}^{\sigma^\pm}(B) = E_X^L(B) \mp \frac{g_X}{2} \mu_B B, \quad (9)$$

where $E_X^L(B)$ is the lowest energy among various L at a certain B to minimise $E_{X-PL}^{\sigma^\pm}(B)$. Also, the theoretical $E_X^L(B)$ can be compared with the measured $E_{X-PL}^{\sigma^\pm}(B)$ as

$$E_X^L(B) = [E_{X-PL}^{\sigma^+} + E_{X-PL}^{\sigma^-}]/2. \quad (10)$$

Likewise, the XX eigenenergy ($E_{XX}^L(B)$) of different exciton orbital angular momenta (L) were obtained as a function of the external magnetic field (B) through an exact diagonalisation method by taking into account the Coulomb interaction amongst the two electrons and two holes. For a XX, our model conserves the electron and hole spins, separately as $\vec{S}_e = \vec{S}_{e1} + \vec{S}_{e2}$ and $\vec{S}_h = \vec{S}_{h1} + \vec{S}_{h2}$. Thus, we can split the 4-particle Hilbert space into 4 sectors, i.e., (electron singlet) \times (hole singlet), (electron singlet) \times (hole triplet), (electron triplet) \times (hole singlet), and (electron triplet) \times (hole triplet). This method drastically reduces calculation costs. For each sector, we used 500 low-lying states to diagonalize the Hamiltonian with the Coulomb interaction. For comparison, we also diagonalized it with 1,000 states, and confirmed that the truncation error in the total energy is less than 0.1%.

When considering the biexciton emission between $E_{XX}^L(B)$ and $E_X^L(B)$, the oscillation period for the minimum $E_{XX}^L(B)$ with B is shorter than that for the minimum $E_X^L(B)$. The selection rule adds a restriction such that the emission only occurs when $E_{XX}^L(B)$ and $E_X^L(B)$ have the same L . For example, when the biexciton energy changes from $E_{XX}^{L=0}$ to $E_{XX}^{L=1}$ with increasing B , $E_X^{L=0}$ is still less than $E_X^{L=1}$. Therefore, an emission between $E_{XX}^{L=1}$ and $E_X^{L=0}$ gives the minimum biexciton PL energy. However, this is not the case. The emission occurs between $E_{XX}^{L=1}$ and $E_X^{L=1}$ due to the selection rules. Consequently, an abrupt decrease of the XX PL energy can be measured at the transition magnetic field, where the biexciton changes its L from 0 to 1.

For an exciton, we found the optimum values for $R_e = 32$ nm, $R_h = 15$ nm, and $W_e = W_h = 5$ nm to reproduce the observed AB oscillation period ($\Delta B_X \sim 1.8$ T). On the other hand, for a biexciton, we found the confinement parameters (R'_e, R'_h, W'_e, W'_h) should be

1.4 times those for exciton. When a single particle is confined, $V_\alpha(r)$ is determined by geometric structure. However, interaction among the N_e electrons and N_h holes can also modify $V_\alpha(r)$ as well as the band gap E_g through the electron-electron and hole-hole repulsion with re-distribution of the surrounding electrons and holes. Therefore, the relatively large values in the parameters (R'_e, R'_h, W'_e, W'_h) effectively describe the modified $V'_{e,h}(r, N_{e,h})$.

We also calculate the two-body densities (Fig.5(a),(b)),

$$\rho_{ee}(x_e|X_e) = \frac{1}{2} \sum_{\sigma, \sigma'} \left\langle \hat{\psi}_{e,\sigma}^\dagger(x_e) \hat{\psi}_{e,\sigma'}^\dagger(X_e) \hat{\psi}_{e,\sigma'}(X_e) \hat{\psi}_{e,\sigma}(x_e) \right\rangle, \quad (11)$$

$$\rho_{hh}(x_h|X_e) = \sum_{\sigma, \sigma'} \left\langle \hat{\psi}_{h,\sigma}^\dagger(x_h) \hat{\psi}_{h,\sigma}(x_h) \hat{\psi}_{e,\sigma'}^\dagger(X_e) \hat{\psi}_{e,\sigma'}(X_e) \right\rangle, \quad (12)$$

that are the probabilities to find an electron at x_e and a hole at x_h , respectively, with an electron fixed at X_e . Here, $\hat{\psi}_{e,\sigma}(x) [\hat{\psi}_{h,\sigma}(x)]$ is the field operator of the electron [hole] with spin σ and position x . We choose X_e at which the electron density has a maximum.

Since excitons are charge neutral, the exciton AB effect requires a difference between the phases acquired by the electron and the hole when the magnetic flux threads the ring. Suppose the electron and the hole in a widthless 1-dimensional (1D) loop are independent or weakly bound through a short-range interaction, optical AB oscillations can be seen in the ground states of the bright exciton, where the total angular momentum of the exciton is kept null as the individual orbital angular momentum of the electron and the hole are canceled ($L = \ell_e + \ell_h = 0$). When a finite width of the ring structure is considered, a quasi 1-dimensional geometric confining potential $V_\alpha(r)$ is obtained, which depends on only ring radius (r) under the assumption of rotational symmetry. In this case, it was known that the ratio of exciton orbit-to-width ($\gamma = R_x/W \geq 1$) is crucial in determining the amplitude of the excitonic AB oscillations. With increasing W , up to R_x in a NQR, the excitonic AB oscillations become suppressed. However, when the e-h pair confined in a finite ring width is strongly bound through a long-range Coulomb interaction, the recent 2D model proposed that the emergence of excitonic AB oscillations is determined by the ring width

and the strain, i.e., the excitonic AB oscillations occur in a limited range of the widths for an isotropic $V_\alpha(r)$. Additionally, the presence of the ring core layer (otherwise the core area is open), plays an important role in enhancing the excitonic AB oscillations via strain effects.

In the case of a strongly bound e-h pair, the 1D model claims that the initial bright exciton ($L = 0$) becomes dark state ($L \neq 0$) with increasing magnetic field, resulting in no excitonic AB oscillation (A. O. Govorov *et al.*, Phys. Rev. B 66, 081309 (2002)). However, this conjecture has not been verified experimentally, for example by looking for emission quenching with increasing magnetic field. In the case of type-II quantum dots, orbital angular momentum is added to the charged single particle rotating in the shell. However, optical AB oscillations were still observed from excitons with non-zero total orbital angular momentum ($L \neq 0$). The exact reason is not clear at the moment. However, regarding the anisotropy of the volcano-like structure, the ideal selection rule for bright and dark exciton states may break down. Therefore, the fine states of the PL spectrum could be described by the mixed states of the spin and orbital angular momentum of bright and dark exciton states.

Supporting information-4: Approximated into a simple 1-dimensional model for excitons and biexcitons

Although our calculation considers the rim width in the quasi 1-dimensional model, we found the strongly correlated states of an electron and a hole in an exciton and also the Wigner molecularisation between two excitons in a biexciton can be approximated into a simplified one-dimensional model. When the ring width is ignored, the effective mass Hamiltonian in Eqs. (1)–(3) for an electron and a hole can be simplified as (A. O. Govorov *et al.*, Phys. Rev.

$$H = \frac{\hbar^2}{2m_e R_e^2} \left(\hat{\ell}_e + \frac{\pi R_e^2 B}{h/e} \right)^2 + \frac{\hbar^2}{2m_h R_h^2} \left(\hat{\ell}_h - \frac{\pi R_h^2 B}{h/e} \right)^2 - \frac{e^2}{4\pi\epsilon} \left[(R_e - R_h)^2 + 4R_e R_h \sin^2 \left(\frac{\theta_e - \theta_h}{2} \right) \right]^{-1/2}, \quad (13)$$

where, θ_e (θ_h) and $\hat{\ell}_e = -i\partial/\partial\theta_e$ ($\hat{\ell}_h = -i\partial/\partial\theta_h$) are the azimuth angle and angular momentum of the electron (hole) respectively, and the Zeeman effect is not included. The center-of-mass and relative coordinates of the exciton are given by

$$\Theta = \frac{m_e R_e^2 \theta_e + m_h R_h^2 \theta_h}{m_e R_e^2 + m_h R_h^2}, \quad \theta = \theta_e - \theta_h. \quad (14)$$

Then, the Hamiltonian in Eq. (13) becomes decoupled as $H = H_{\text{CM}} + H_{\text{rel}}$,

$$H_{\text{CM}} = \frac{\hbar^2}{2m_X R_X^2} \left[\hat{L} + \frac{\pi(R_e^2 - R_h^2)B}{h/e} \right]^2, \quad (15)$$

$$H_{\text{rel}} = \frac{\hbar^2}{2\mu R_{\text{rel}}^2} \left(\hat{\ell} + \frac{\pi R_{\text{rel}}^2 B}{h/e} \right) - \frac{e^2}{4\pi\epsilon} \left[(R_e - R_h)^2 + 4R_e R_h \sin^2 \frac{\theta}{2} \right]^{-1/2}, \quad (16)$$

with $R_X^2 = (m_e R_e^2 + m_h R_h^2)/(m_e + m_h)$, $R_{\text{rel}} = R_e R_h / R_X$, and $m_X = m_e + m_h$. We have introduced the total angular momentum $\hat{L} = \hat{\ell}_e + \hat{\ell}_h = -i\partial/\partial\Theta$ and relative angular momentum $\hat{\ell} = \frac{m_h R_h^2 \hat{\ell}_e - m_e R_e^2 \hat{\ell}_h}{m_e R_e^2 + m_h R_h^2} = -i\partial/\partial\theta$. The energy eigenstates can be given as $\Psi_{X,L}(\theta_e, \theta_h) = e^{iL\Theta} \psi_{X,L}(\theta)$ with L ($= 0, \pm 1, \pm 2, \dots$). We see that the center-of-mass and relative motion are not completely decoupled; $\Psi_L(\theta_e, \theta_h) = \Psi_L(\theta_e \pm 2\pi, \theta_h) = \Psi_L(\theta_e, \theta_h \pm 2\pi)$, and an unusual boundary condition for $\psi_L(\theta)$ is given by

$$\psi_L(\theta \pm 2\pi) = \exp \left[\pm i 2\pi L \frac{m_e R_e^2}{m_e R_e^2 + m_h R_h^2} \right] \psi_L(\theta). \quad (17)$$

The low-lying states of an exciton can be estimated by using the harmonic approximation. By expanding the Coulomb interaction up to θ^2 , we obtain $\psi_{X,L}(\theta) \propto \exp\{-\theta^2/(2\xi_X^2)\}$ with

the “localization length” defined by

$$\xi_X = \left[\frac{a_B R_X^2 |R_e - R_h|^3}{(R_e R_h)^3} \right]^{1/4}. \quad (18)$$

As $\xi_X \sim 0.64$ in our system is sufficiently small compared to π , the harmonic approximation can be justified. This indicates that the electron and the hole are strongly correlated to each other, and move together with $\theta_e \simeq \theta_h$, as schematically shown in S-Fig. 2(a). The low-lying energies can also be approximated as

$$E_X(L) = \frac{\hbar^2}{2m_X R_X^2} \left[L + \frac{\pi(R_e^2 - R_h^2)B}{h/e} \right]^2 + \text{const.}, \quad (19)$$

which is in agreement with the recent 1-dimensional model (A. O. Govorov *et al.*, Phys. Rev. B 66, 081309 (2002)).

On the other hand, for a biexciton, instead of two electrons and two holes, we consider two excitons as point particles that move in the ring, as shown in Supplementary Fig. 2(b). Suppose a ring orbit radius R'_X is given for the exciton, the electric dipole of j -th exciton can be defined as $-e(R'_e - R'_h)r_j/R'_0$, where r_j is its position measured from the ring center. Therefore, the effective Hamiltonian for two excitons with the dipole-dipole interaction can be given by

$$H = \sum_{j=1}^2 \frac{\hbar^2}{2m_X R_X'^2} \left[\hat{\ell}_j + \frac{\pi(R_e'^2 - R_h'^2)B}{h/e} \right]^2 + \frac{e^2(R'_e - R'_h)^2}{4\pi\epsilon R_X'^3} \frac{1 + \sin^2 \frac{\theta_1 - \theta_2}{2}}{8 |\sin^3 \frac{\theta_1 - \theta_2}{2}|}. \quad (20)$$

The dipole-dipole interaction becomes minimised when $|\theta_1 - \theta_2| = \pi$, i.e., the two excitons are located at opposite sides of the ring. In a similar case to that used for the exciton, the harmonic approximation enables us to estimate the wavefunction of the biexciton (or interacting two exciton dipoles) in relative coordinates as $\psi_{XX,L}(\theta_1 - \theta_2) \propto \exp[-(|\theta_1 - \theta_2| -$

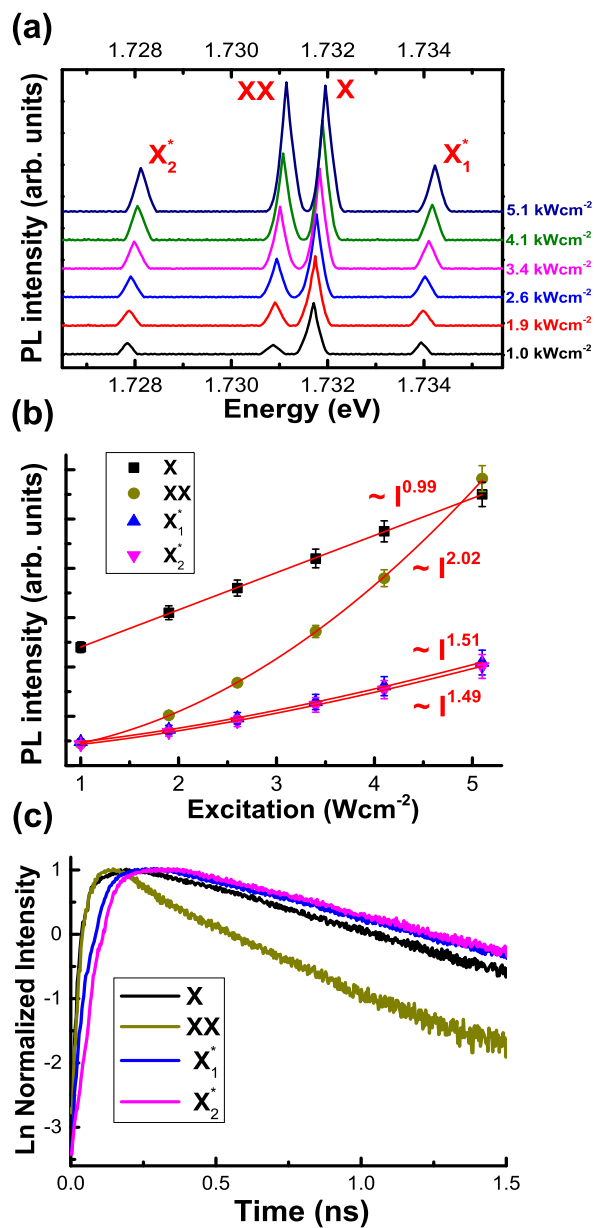
$\pi)^2/(2\xi_{\text{XX}}^2)]$ ($|\theta_1 - \theta_2| < 2\pi$). Since the “localization length” of the biexciton,

$$\xi_{\text{XX}} = \left[\frac{64}{5} \frac{\mu}{m_{\text{X}}} \frac{a_{\text{B}} R'_{\text{X}}}{(R'_{\text{e}} - R'_{\text{h}})^2} \right]^{1/4} \sim 0.91, \quad (21)$$

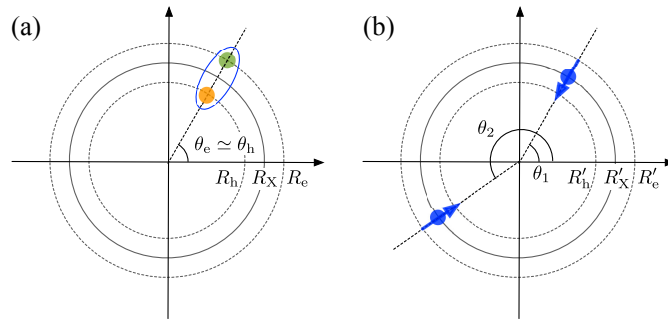
is smaller than π , the harmonic approximation is still valid again. Likewise, the low-lying energy of the biexciton can be approximated as

$$E_{\text{XX}}(L) = \frac{\hbar^2}{2(2m_{\text{X}})R'_{\text{X}}{}^2} \left[L + 2 \frac{\pi(R'_{\text{e}}{}^2 - R'_{\text{h}}{}^2)B}{h/e} \right]^2 + \text{const.} \quad (22)$$

This equation suggests the biexciton can be treated as a single particle with twice the exciton mass (m_{X}). Indeed, when the dipole-dipole interaction becomes minimised with $|\theta_1 - \theta_2| = \pi$, the distance between the two excitons becomes maximised. This condition indicates the formation of a Wigner molecule from the two excitons (R. Okuyama *et al.*, Phys. Rev. B 83, 195311 (2011)).



S-Fig. 1: (a) As the excitation power increases, biexcitons (XX) and charged excitons (X_1^* and X_2^*) emerge near the neutral exciton (X) in the PL spectrum, which can be identified by measuring the integrated PL intensity as a function of excitation power (b) and by time-resolved PL (c).



S-Fig. 2: (a) Schematic view of the low-lying states of an exciton in a quantum ring. An electron and a hole are strongly coupled to each other, and they move together with $\theta_e \simeq \theta_h$. (b) Simplified model of a biexciton in the ring, where each exciton is treated as a point particle with a radial electric dipole moment.